Toward convergence of effective-field-theory simulations on digital quantum computers

O. Shehab, K. Landsman, Y. Nam, D. Zhu, N. M. Linke, M. Keesan, R. C. Pooser, and C. Monroe

Toward convergence of effective field theory simulations on digital quantum computers

O. Shehab,[1] K. Landsman,[2] Y. Nam,[1] D. Zhu,[2] N. M. Linke,[2] M. Keesan,[1] R. C. Pooser,[3, 4] and C. Monroe[2, 1]

[1]*IonQ, Inc, 4505 Campus Drive College Park, MD 20740, USA*
[2]*Joint Quantum Institute, Department of Physics and Joint Center for Quantum Information and Computer Science,*
University of Maryland, College Park, MD 20742
[3]*Computational Sciences and Engineering Division,*
Oak Ridge National Laboratory, Oak Ridge, TN 37831, USA
[4]*Department of Physics and Astronomy, University of Tennessee, Knoxville, TN 37996, USA*
(Dated: November 22, 2019)

We report results for simulating an effective field theory to compute the binding energy of the deuteron nucleus using a hybrid algorithm on a trapped-ion quantum computer. Two increasingly complex unitary coupled-cluster ansaetze have been used to compute the binding energy to within a few percent for successively more complex Hamiltonians. By increasing the complexity of the Hamiltonian, allowing more terms in the effective field theory expansion and calculating their expectation values, we present a benchmark for quantum computers based on their ability to scalably calculate the effective field theory with increasing accuracy. Our result of $E_4 = -2.220 \pm 0.179 \text{MeV}$ may be compared with the exact Deuteron ground-state energy -2.224MeV. We also demonstrate an error mitigation technique using Richardson extrapolation on ion traps for the first time. The error mitigation circuit represents a record for deepest quantum circuit on a trapped-ion quantum computer.

I. INTRODUCTION

Simulating Fermionic matter using quantum computers has recently become an active field of research. With the advent of noisy intermediate-scale quantum (NISQ) devices that are capable of processing quantum information, hybrid quantum-classical computing (HQCC) has been proposed to be a worthy strategy to harness the advantage quantum computers provide as early as possible. A host of HQCC demonstrations, ranging from its application in chemistry [1–4] to machine learning [5], are in fact already available in the literature.

NISQ devices are however susceptible to errors and defects. Thus, the quantum circuits to be run on these machines need to be sufficiently small so that the results that the quantum computers output are still useful. On the other hand, in order for the quantum computational results to be useful, the computation that the quantum computer performs needs to be sufficiently demanding such that readily available classical devices cannot easily arrive at the same results. However, there is a lack of empirical evidence for the performance scaling of HQCC as problems become more complex. A test, or benchmark, of this scalability would be useful to inform future quantum algorithm development.

Here, using the effective field theory (EFT) simulation of a deuteron, first introduced in [3], we outline a path to scalable HQCC and provide a benchmark that determines the HQCC performance scaling of a quantum computer. We further demonstrate that a trapped-ion quantum computer today is capable of addressing small, yet scalable HQCC problems, and that it shows promises toward scaling to reliable computational results when a quantum advantage is demonstrated.

We also demonstrate a re-parametrization technique that yields a quantum circuit amenable to implementation on quantum computers with nearest-neighbor connectivity. We report our experimental results that leverage known error mitigation techniques [6–9]. The theoretical predictions for the three- and four-qubit case are within the error bars of the experimental results.

II. HAMILTONIAN AND ANSATZ

The N oscillator-basis deuteron Hamiltonian considered in [3] (see Supplementary material for detail) is

$$H_N = \sum_{n,n'=0}^{N-1} \langle n'|(T+V)|n\rangle a_{n'}^\dagger a_n, \qquad (1)$$

where the operators $a_n^\dagger$ and a_n create and annihilate a deuteron in the harmonic-oscillator s-wave state $|n\rangle$ and the matrix elements of the kinetic and potential energy are

$$\langle n'|T|n\rangle = \frac{\hbar\omega}{2}\left[(2n+3/2)\delta_n^{n'} - \sqrt{n(n+1/2)}\delta_n^{n'+1}\right.$$
$$\left. -\sqrt{(n+1)(n+3/2)}\delta_n^{n'-1}\right],$$
$$\langle n'|V|n\rangle = V_0\delta_n^0\delta_n^{n'}, \qquad (2)$$

where $\hbar\omega = 7\,\text{MeV}$ [3] and $V_0 = 5.68658111\,\text{MeV}$ [10]. Since our goal is to find the ground state energy expectation values as a function of N using a quantum computer, we apply Jordan-Wigner transform [11] to our physical Hamiltonian in (1) to find the qubit Hamiltonian. For $N = 2, 3$, and 4, we have

$$H_2 = 5.907I + 0.218Z_0 - 6.125Z_1 - 2.143(X_0X_1 + Y_0Y_1)$$
$$H_3 = H_2 + 9.625(I - Z_2) - 3.913(X_1X_2 + Y_1Y_2)$$
$$H_4 = H_3 + 13.125(I - Z_3) - 5.671(X_2X_3 + Y_2Y_3). \qquad (3)$$

For our current example of a Deuteron EFT simulation, the UV cutoff determines the largest matrix element in the nuclear Hamiltonian, which controls the scaling of the coefficients of the Pauli terms in the qubit Hamiltonian in (3). Since the uncertainty in determining the expectation value of the Hamiltonian is bounded by the largest absolute value of the coefficients in the qubit Hamiltonian [2], the higher the UV cutoff, the larger the uncertainty in the expectation value of the Hamiltonian becomes. To meet the required, preset uncertainty, we need to make a larger number of measurements for a large-coefficient Hamiltonian. Because the largest coefficient tends to grow with basis size, this effectively induces an implementation-level tug-of-war between the increasingly accurate simulation from considering a larger oscillator basis and the accumulation of errors on NISQ devices susceptible to, e.g., drifts, that occur over the required, longer overall runtime. While frequently calibrating the quantum computer may help reduce the errors, this may not be desirable as it would significantly increase the resource overhead.

For the HQCC ansatz, we use the N-site unitary coupled-cluster singles (UCCS) ansatz [12]

$$|\Psi_{\mathrm{UCCS}}\rangle = \exp\left(\sum_{k=1}^{N-1} \theta_k [a_0^\dagger a_k - a_k^\dagger a_0]\right)|1_0\rangle, \quad (4)$$

where $\vec{\theta} = \{\theta_1, ..., \theta_{N-1}\}$ is the set of $N-1$ real-valued variational parameters and $|1_i\rangle$ denotes the state $|0, ..., 0, 1, 0, ..., 0\rangle$ with the ith s-wave state occupied. We compute the deuteron binding energy by minimizing the quantum functional $\langle\Psi_{\mathrm{UCCS}}|H_N|\Psi_{\mathrm{UCCS}}\rangle$ with respect to $\vec{\theta}$. The initial state $|1_0\rangle = |1, 0, 0, ...0\rangle$ represents the occupation of the 0th s-wave state.

To implement the UCCS ansatz on our quantum computer, we re-parameterized (4) in the hyper-spherical coordinate [12, 13], i.e.,

$$|\Psi_{\mathrm{UCC}}\rangle = \sum_{k=0}^{N-2} \cos(\lambda_k)|\tilde{1_k}\rangle + |\tilde{1_{N-1}}\rangle, \quad (5)$$

where $|\tilde{1_k}\rangle \equiv \prod_{i=0}^{k-1}\sin(\lambda_i)|1_k\rangle$ with $|\tilde{1_0}\rangle = |1_0\rangle$. This choice is deliberate and exact, since the excitation operator in (4) is solely composed of single-excitations. Note we have relabeled (and re-indexed) variational parameters as $\vec{\lambda} = \{\lambda_0, ..., \lambda_{N-2}\}$.

With the new parameterization shown in (5), we may now synthesize the ansatz circuit straightforwardly. Let us define the amplitude shifting unitary $U_{i,i+1}(\lambda_i) \equiv (C_{i+1}X_i)(C_i RY_{i+1}(\lambda_i))$, where $C_m G_n$, for instance, denotes a single-qubit gate G acting on qubit n, controlled by qubit m, such that $U(\lambda)(\alpha|00\rangle + \beta|10\rangle) = \alpha|00\rangle + \beta(\cos\lambda|10\rangle + \sin\lambda|01\rangle)$. Applying $U_{i,i+1}$ in series to an initial state of $|1_0\rangle$, we have

$$|\Psi_{\mathrm{UCC}}\rangle = \left[\prod_{i=0}^{N-2} U_{i,i+1}(\lambda_i)\right]|1_0\rangle. \quad (6)$$

For the first non-trivial case of $N = 2$, we need to optimize $U_{0,1}$ acting on $|1_0\rangle$. Since the initial state is $|10\rangle$, $C_0 iRY_1|10\rangle = iRY_1|10\rangle$. The optimized circuit $\mathcal{C}_2$ is
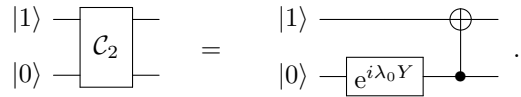
For $N > 2$, we iteratively construct the circuit $\mathcal{C}_N$ as shown below.
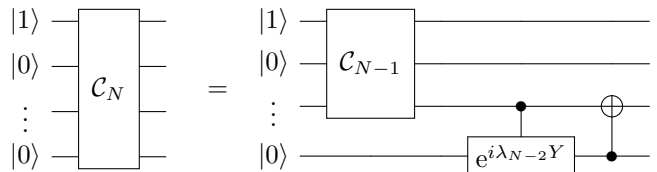
III. RESULTS

We implemented our EFT simulation on an ion-trap quantum computer that may selectively load either five or seven ^{171}Yb$^+$ qubits. The qubit states $|0\rangle = |0, 0\rangle$ and $|1\rangle = |1, 0\rangle$ (with quantum numbers $|F, m_F\rangle$) are chosen from the hyperfine-split ^{2}S$_{1/2}$ ground level with an energy difference of 12.64 GHz. The T_2 coherence time with idle qubits is measured to be 1.5(5) sec, limited by residual magnetic field noise. The ions are initialized by an optical pumping scheme and are collectively read out using state-dependent fluorescence detection [14], with each ion being mapped to a distinct photomultiplier tube (PMT) channel. State detection and measurement (SPAM) errors are characterized and corrected for in detail by inferring the state-to-state error matrix [15].

For the details of the single and two qubit gate implementations we refer the readers to Appendix A of [16] and to [17–20]. For the three qubit ansatz, we load five ions in the trap and use every other ion as qubit. For the four qubit ansatz, we load seven ions in the trap, using the inner 5 as qubits, with the outermost pair being used to evenly space the middle five ions. Entangling gates are derived from normal motional modes that result from the Coulomb interaction between ions, and the trapping potential. Off-resonantly driving both red and blue motional modes simultaneously leads to an entangling Mølmer-Sørensen interaction [18].(See Supplementary material for circuits optimized for the native gate set.)

In the three qubit experiment, the logical qubits $1, 2, 3$, that denote s-wave states, are mapped to physical qubits $3, 1, 5$. In the four qubit experiment, the logical qubits $1, 2, 3, 4$ are mapped to the physical qubits $1, 2, 3, 5$. The single qubit rotation fidelities are ~ 0.995 for each ion. The two qubit gate fidelity is given by the measured probabilities P_{00} and P_{11} of states $|00\rangle$ and $|01\rangle$, respectively and the contrast Π_c of the parity curve. The fidelity of our operations is characterized using a widely used proxy,

the fidelity of producing a Bell state from a separable state. The fidelity expression is $F = (P_{00} + P_{11} + \Pi_c)/2$ [21]. The two qubit gate fidelities of the system are 0.986(2), 0.969(8), 0.993(6), 0.980(9), and 0.992(7) for the qubit pairs $(1,3)$, $(1,5)$, $(3,5)$, $(1,2)$, and $(2,3)$ respectively [21, 22]. Readout error sources (crosstalk, dark count, off-resonant pumping, etc) are measured simultaneously by preparing a single ion in either the bright or dark state and moving it under different PMT channels [15]. The errors for different multi-qubit states are generated by looking at photon counts from the entire array of PMT channels and aggregating data appropriately. By characterizing the imaging and detection system with a single ion we estimate that the mean detection fidelity over all bit strings for three and four qubit experiments are are 0.978 and 0.963 respectively [22, 23].

Figure 1 shows the experimentally determined expectation value of the Hamiltonian H_3 at the theoretically predicted minimum $\lambda_0 = 0.250$ and $\lambda_1 = 0.830$. We employed the error minimization technique [8, 9], based on Richardson extrapolation [24], to our circuit by replacing all occurrences of $XX(\theta)$ with $XX(\theta)\mathbb{1}^M$, where $\mathbb{1}^M = [XX(-\theta)XX(\theta)]^M$ for $M = 0, 1, 2, 3$. The linearly-extrapolated, zero-noise limit shows $\langle H_3 \rangle = -2.030 \pm 0.034$MeV, which is in excellent agreement with the theoretically expected value of -2.046MeV.

Figure 2 shows the analogous figure for H_4 evaluated at the theoretically optimal parameters $\lambda_0 = 0.8584$, $\lambda_1 = 0.9584$, and $\lambda_2 = 0.7584$. The linearly-extrapolated, zero-noise limit shows $\langle H_4 \rangle = -2.220 \pm 0.179$MeV, again statistically consistent with the theoretically expected value of -2.143MeV. We note that the largest circuit that was run on our quantum computer to generate Figure 2 involved implementing 35 two-qubit XX gates. We observe that the curve for the expectation value of the Hamiltonian in our plots are flatter than that of Fig. 3 of [3] which indicates lower error rates in our device.

To further corroborate the accuracy of our quantum computational results, we also investigated the energy expectation values at various locations in the ansatz parameter space. Specifically, we explored the four-qubit ansatz's parameter settings that theoretically result in approximately 10% or 20% deviation from the theoretical minimum by varying one parameter at a time while fixing the other two constant to their optimal values. Table I shows the choice of parameters and their respective, experimentally-obtained zero-noise-limit expectation values of H_4, compared with the theoretical values. We
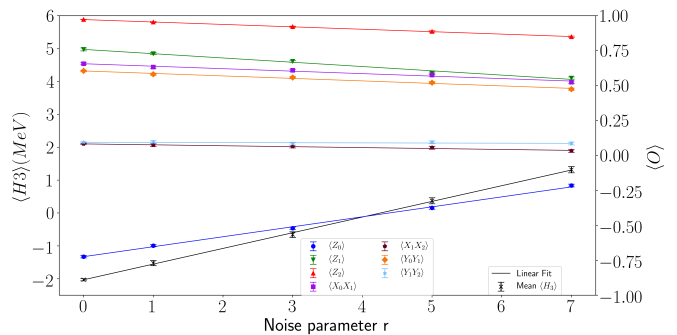

FIG. 1. Expectation values of Hamiltonian terms in H_3 as a function of noise parameter $r = 2M + 1$ which is the number of repetitions of noisy two qubit identity gates before a given two qubit gate. M is defined in the Results section. Various colored, solid symbols are the expectation values of individual terms in H_3. Black crosses are H_3, computed according to Eq. (3). Colored, solid lines are the linear fits to the corresponding individual Hamiltonian terms in H_3. The black solid line is the linear fit to H_3. We use the linear fits to extrapolate to the zero noise limit. The error bars in the figure are statistical errors based on finite sampling and a binomial distribution. The binding energy is determined as -2.030 ± 0.034MeV
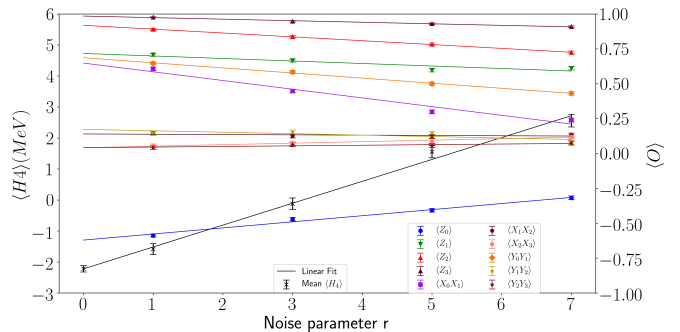

FIG. 2. Expectation values of Hamiltonian terms in H_4 as a function of noise parameter $r = 2M + 1$ which is the number of repetitions of noisy two qubit identity gates before a given two qubit gate. M is defined in the Results section. Various colored, solid symbols are the expectation values of individual terms in H_4. Black crosses are H_4, computed according to Eq. (3). Colored, solid lines are the linear fits to the corresponding individual Hamiltonian terms in H_4. The black solid line is the linear fit to H_4. We use the linear fits to extrapolate to the zero noise limit. The error bars in the figure are statistical errors based on finite sampling and a binomial distribution. The binding energy is determined as -2.220 ± 0.179MeV.

show in Fig. 3 the data reported in Table I as a visual aid. The minimal binding energy can be estimated by fitting each set of data to a quadratic form and minimizing the fit. Doing so results in individual estimates of $E_i = -2.080 \pm -0.151, -2.200 \pm 0.149, -1.946 \pm 0.124$, for the three respective lambda parameters, with an average minima of $E = -2.088$ with 2.9% error. Our computations therefore match previous error rates while increasing the system size, thus continuing to provide a path

λ_0	λ_1	λ_2	$\langle H_4\rangle$[experiment]	$\langle H_4\rangle$[theory]
0.858	0.958	0.758	-2.256 ± 0.179	-2.143
0.420	0.958	0.758	-1.568 ± 0.165	-1.693
0.550	0.958	0.758	-1.708 ± 0.172	-1.925
1.140	0.958	0.758	-1.492 ± 0.190	-1.921
1.260	0.958	0.758	-1.599 ± 0.191	-1.708
0.858	0.190	0.758	-1.425 ± 0.169	-1.707
0.858	0.410	0.758	-1.549 ± 0.172	-1.916
0.858	1.440	0.758	-2.064 ± 0.187	-1.915
0.858	1.630	0.758	-1.646 ± 0.188	-1.707
0.858	0.958	-0.510	-2.066 ± 0.179	-1.713
0.858	0.958	-0.120	-1.370 ± 0.182	-1.917
0.858	0.958	1.600	-1.524 ± 0.187	-1.918
0.858	0.958	1.930	-1.563 ± 0.194	-1.709

TABLE I. Expectation value $\langle H_4\rangle$ for various sets of variational parameters. $\langle H_4\rangle$[experiment] denote the zero-noise limit extrapolated values of $\langle H_4\rangle$ obtained from our trapped-ion quantum computer. $\langle H_4\rangle$[theory] denote the corresponding, theoretically predicted values. All energies are measured in MeV. The top row shows the exact minimum configuration and results. The next set of four rows show the cases where we vary λ_0. The following two sets of four rows show the corresponding configuration-results pair for varying λ_1 and λ_2, respectively.
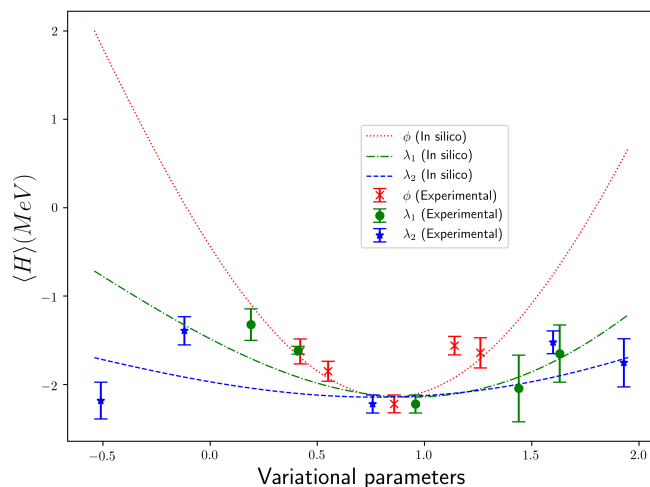

FIG. 3. Expectation value $\langle H_4\rangle(r=0)$ as a function of a parameter chosen from the set $\{\lambda_0, \lambda_1, \lambda_2\}$. The plot symbols denote the zero-noise-limit extrapolated from the experimental data, also given in Table I, and the solid lines denote the theoretical values.

towards scalable simulations.

IV. DISCUSSION

In this paper, we show the quantum computational results obtained from 5- and 7-qubit trapped-ion quantum computers simulating a Deuteron. We improved on the previous result for the three-qubit ansatz and extended the ansatz size beyond the previous state of the art [3]. We construct physically optimized circuits specifically for
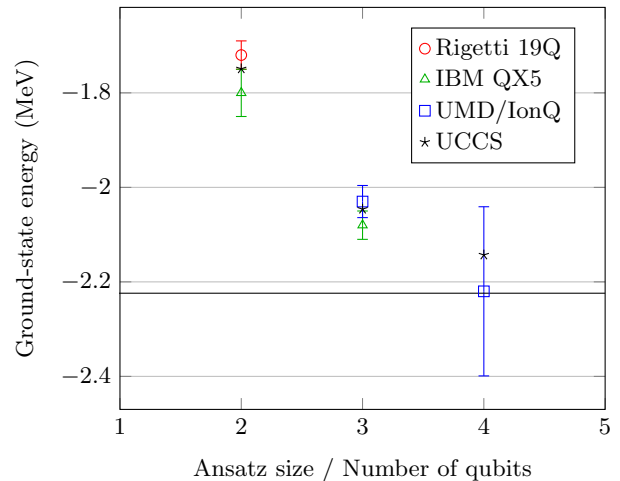

FIG. 4. Aggregate results on the Deuteron simulation performed across different quantum computing platforms. Open symbols denote the experimental results. Star symbols denote the exact UCCS results. The black solid line denotes the exact deuteron ground-state energy. We note that the results on other platform has been determined variationally on the hardware.

trapped-ion architecture. A native and more efficient implementation of the circuit for Richardson extrapolation is also presented. Our four-qubit ansatz result of $E_4 = -2.220 \pm 0.179$MeV may be compared with the exact Deuteron ground-state energy -2.224MeV. The wider error bar for the four qubit result is not an effect of the algorithmic approach we have taken here. Rather it is the result of the two qubit gate error on the hardware. We believe there are research pathways to bring this error down which will hopefully make the scalability of our approach even more obvious.

Figure 4 shows the aggregate results, collected from previous studies performed on different quantum computing platforms on the same Deuteron system [3] and our own results. For the three qubit ansatz, the error margin of the binding energy computed on the IBM QX5 was 3%, while it is 0.7% on the IonQ-UMD trapped ion quantum computer at the optimal configuration for the three qubit experiment. Because of the demanding size of the circuit and the susceptibility of NISQ devices to errors, we were unable to run the four-qubit experiments on other quantum computing platforms. We find that, based on Fig. 4, the simulation results converge to the known ground state energy as a function of the ansatz size. We also note that, as expected, the experimental results start deviating more from the exact UCCS results, due to the accumulation of errors.

It is important to point out that single excitations are in principle much easier to simulate, and therefore will not themselves be a good measure of quantum advantage going forward as quantum computers grow. More complex EFTs, such as for more massive Helium nuclei (with more orbitals and more excitations) will stress fu-

ture quantum computer hardware more comprehensively. We are currently studying the implementation of many body EFT on NISQ devices. The present single body problem lays the groundwork for future EFT simulations on ion trap hardware. Thus, we believe that our EFT simulation may be used as a practical benchmark for quantum computers which characterizes the performance of HQCC algorithms in the presence of noise, alongside the known proposals [5, 25]. We have already successfully implemented the simulation across different platforms (superconducting and trapped-ion quantum computers) and also within the same platform with different configurations (5 and 7 qubit trapped-ion quantum computers). Since our ansatz circuits require only nearest-neighbor connectivity, our benchmark is expected to be readily be implemented across any platform and serve as a baseline, since more complex connectivity available on a quantum computer can only help boost the quantum computational power [26]. Our HQCC approach will also help benchmark the interface between quantum and classical processors. In this paper, we have taken first steps in this direction. We anticipate using the algorithm to benchmark upcoming quantum information processors.

V. ACKNOWLEDGMENTS

[1] P. J. J. O'Malley, R. Babbush, I. D. Kivlichan, J. Romero, J. R. McClean, R. Barends, J. Kelly, P. Roushan, A. Tranter, N. Ding, B. Campbell, Y. Chen, Z. Chen, B. Chiaro, A. Dunsworth, A. G. Fowler, E. Jeffrey, E. Lucero, A. Megrant, J. Y. Mutus, M. Neeley, C. Neill, C. Quintana, D. Sank, A. Vainsencher, J. Wenner, T. C. White, P. V. Coveney, P. J. Love, H. Neven, A. Aspuru-Guzik, and J. M. Martinis, Scalable quantum simulation of molecular energies, Phys. Rev. X **6**, 031007 (2016).

[2] A. Kandala, A. Mezzacapo, K. Temme, M. Takita, M. Brink, J. M. Chow, and J. M. Gambetta, Hardware-efficient variational quantum eigensolver for small molecules and quantum magnets, Nature **549**, 242 (2017), arXiv:1704.05018.

[3] E. F. Dumitrescu, A. J. McCaskey, G. Hagen, G. R. Jansen, T. D. Morris, T. Papenbrock, R. C. Pooser, D. J. Dean, and P. Lougovski, Cloud quantum computing of an atomic nucleus, Phys. Rev. Lett. **120**, 210501 (2018).

[4] Y. Nam, J.-S. Chen, N. C. Pisenti, K. Wright, C. Delaney, D. Maslov, K. R. Brown, S. Allen, J. M. Amini, J. Apisdorf, K. M. Beck, A. Blinov, V. Chaplin, M. Chmielewski, C. Collins, S. Debnath, A. M. Ducore, K. M. Hudek, M. Keesan, S. M. Kreikemeier, J. Mizrahi, P. Solomon, M. Williams, J. D. Wong-Campos, C. Monroe, and J. Kim, Ground-state energy estimation of the water molecule on a trapped ion quantum computer, arXiv:1902.10171 (2019).

[5] M. Benedetti, D. Garcia-Pintos, O. Perdomo, V. Leyton-Ortega, Y. Nam, and A. Perdomo-Ortiz, A generative modeling approach for benchmarking and training shallow quantum circuits, , arXiv:1801.07686 (2018).

[6] K. Temme, S. Bravyi, and J. M. Gambetta, Error mitigation for short-depth quantum circuits, Physical Review Letters **119**, 180509 (2017).

[7] Y. Li and S. C. Benjamin, Efficient variational quantum simulator incorporating active error minimization, Physical Review X **7**, 021050 (2017).

[8] S. Endo, S. C. Benjamin, and Y. Li, Practical quantum error mitigation for near-future applications, Physical Review X **8**, 031027 (2018).

[9] S. McArdle, X. Yuan, and S. Benjamin, Error mitigated quantum computational chemistry, arXiv:1807.02467 (2018).

[10] S. König, S. Bogner, R. Furnstahl, S. More, and T. Papenbrock, Ultraviolet extrapolations in finite oscillator bases, Physical Review C **90**, 064007 (2014).

[11] P. Jordan and E. P. Wigner, über das paulische äquivalenzverbot, in *The Collected Works of Eugene Paul Wigner* (Springer, 1993) pp. 109–129.

[12] H.-H. Lu, N. Klco, J. M. Lukens, T. D. Morris, A. Bansal, A. Ekström, G. Hagen, T. Papenbrock, A. M. Weiner, M. J. Savage, and P. Lougovski, Simulations of subatomic many-body physics on a quantum frequency processor, arXiv:1810.03959 (2018).

[13] A. Bansal, S. Binder, A. Ekström, G. Hagen, G. R. Jansen, and T. Papenbrock, Pion-less effective field theory for atomic nuclei and lattice nuclei, Physical Review C **98**, 054301 (2018).

[14] S. Olmschenk, K. Younge, D. Moehring, D. Matsukevich, P. Maunz, and C. Monroe, Manipulation and detection of a trapped yb+ hyperfine qubit, Physical Review A **76**, 052314 (2007).

[15] A. H. Burrell, *High fidelity readout of trapped ion qubits*, Ph.D. thesis, University of Oxford, UK (2010).

[16] K. A. Landsman, C. Figgatt, T. Schuster, N. M. Linke, B. Yoshida, N. Y. Yao, and C. Monroe, Verified quantum information scrambling, arXiv:1806.02807 (2018).

[17] S. Debnath, N. M. Linke, C. Figgatt, K. A. Landsman, K. Wright, and C. Monroe, Demonstration of a small

programmable quantum computer with atomic qubits, Nature **536**, 63 (2016).

[18] K. Mølmer and A. Sørensen, Multiparticle entanglement of hot trapped ions, Physical Review Letters **82**, 1835 (1999).

[19] S.-L. Zhu, C. Monroe, and L.-M. Duan, Arbitrary-speed quantum gates within large ion crystals through minimum control of laser beams, EPL (Europhysics Letters) **73**, 485 (2006).

[20] T. Choi, S. Debnath, T. Manning, C. Figgatt, Z.-X. Gong, L.-M. Duan, and C. Monroe, Optimal quantum control of multimode couplings between trapped ion qubits for scalable entanglement, Physical Review Letters **112**, 190502 (2014).

[21] K. Kim, M.-S. Chang, R. Islam, S. Korenblit, L.-M. Duan, and C. Monroe, Entanglement and tunable spin-spin couplings between trapped ions using multiple transverse modes, Physical Review Letters **103**, 120502 (2009).

[22] S. Debnath, *A programmable five qubit quantum computer using trapped atomic ions*, Ph.D. thesis (2016).

[23] C. Figgatt, D. Maslov, K. Landsman, N. M. Linke, S. Debnath, and C. Monroe, Complete 3-qubit grover search on a programmable quantum computer, Nature communications **8**, 1918 (2017).

[24] L. F. Richardson, B. J Arthur Gaunt, *et al.*, Viii. the deferred approach to the limit, Phil. Trans. R. Soc. Lond. A **226**, 299 (1927).

[25] A. W. Cross, L. S. Bishop, S. Sheldon, P. D. Nation, and J. M. Gambetta, Validating quantum computers using randomized model circuits, arXiv:1811.12926 (2018).

[26] N. M. Linke, D. Maslov, M. Roetteler, S. Debnath, C. Figgatt, K. A. Landsman, K. Wright, and C. Monroe, Experimental comparison of two quantum computing architectures, Proceedings of the National Academy of Sciences **114**, 3305 (2017).